IEEE Photonics Journal
An IEEE Photonics Society Publication

Open Access

Nanoimprint Fabrication of Slot Waveguides

Volume 5, Number 2, April 2013

Marianne Hiltunen
Esa Heinonen
Jussi Hiltunen
Jarkko Puustinen
Jyrki Lappalainen
Pentti Karioja

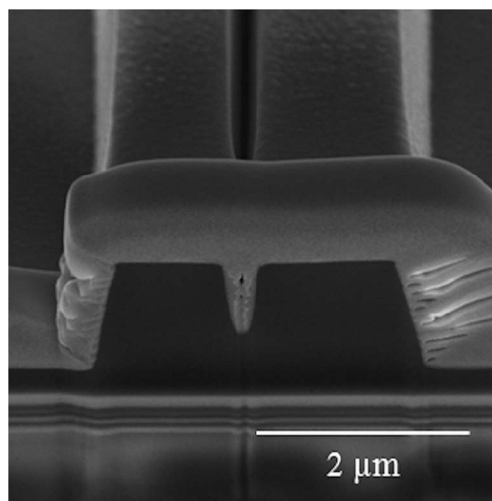

DOI: 10.1109/JPHOT.2013.2251876
1943-0655/$31.00 ©2013 IEEE

IEEE photonics SOCIETY

IEEE

Nanoimprint Fabrication of Slot Waveguides

Marianne Hiltunen,[1] Esa Heinonen,[2] Jussi Hiltunen,[1] Jarkko Puustinen,[3] Jyrki Lappalainen,[3] and Pentti Karioja[1]

[1]VTT Technical Research Centre of Finland, 90570 Oulu, Finland
[2]Center of Microscopy and Nanotechnology, University of Oulu, 90014 Finland
[3]Department of Electrical and Information Engineering, Microelectronics and Materials Physics Laboratories, University of Oulu, 90014 Finland

DOI: 10.1109/JPHOT.2013.2251876
1943-0655/$31.00 ©2013 IEEE

Manuscript received February 5, 2013; revised March 1, 2013; accepted March 2, 2013. Date of publication March 8, 2013; date of current version March 15, 2013. This work was supported by the Finnish Academy under Grants 137331 (M. H.) and 133814 (J. H.). Corresponding author: M. Hiltunen (e-mail: Marianne.Hiltunen@vtt.fi).

Abstract: A nanoimprint mold for optical waveguide applications was fabricated by combining photolithography and focused ion beam (FIB) milling. The feasibility of the proposed method was demonstrated by imprinting 15-mm-long Y-branch waveguides, which had nanoscale slots embedded in one arm. Structural analysis of the FIB milled region showed surface roughness values below 2.5 nm. Characterization of the fabricated waveguides proved that 44% of the optical power was transmitted through the slot-embedded waveguide arm. Operation of slot waveguide was demonstrated at a wavelength of 1305 nm using Young interferometer devices.

Index Terms: Waveguides, subwavelength structures, fabrication and characterization.

1. Introduction

In nanoimprint lithography (NIL), the surface–relief features of a mold are transferred to a polymer resist by mechanical replication [1]. Pattern deformation can be based on thermal embossing or ultraviolet (UV) curing of a liquid-phase polymer. Large-area patterns in a nanoimprint mold are typically processed lithographically, for example, using UV-photolithography or electron-beam lithography, followed by a reactive ion etching step. The direct writing focused ion beam (FIB) method has been used to fabricate small-area stamps for NIL or for repairing NIL stamps [2], [3]. FIB writing is a favorable direct writing method in terms of resolution and accuracy. The resolution in the sub-10-nm range is achievable with FIB milling. However, the processing time is the main limitation of the method. The processing times of dimensions above 100 μm begin to become unacceptably high [4].

It is typical of the integrated optical devices that the length of the waveguides is in the order of centimeters. Due to the replication nature of the imprinting, the quality of the mold has to be very high, particularly when fabricating long waveguides with good transmission properties. The smoothness of the patterns, in particular, is of great importance in optical waveguide devices. Photolithography has been shown to be a good option for preparing molds for the imprint fabrication of long waveguides with low surface roughness [5], [6]. However, feature sizes in the shadow-mask photolithography method are restricted by the wave diffraction, and therefore, this method is applicable to fabricate micron-scale and larger features. In modern integrated optics, there is an increasing need for embedding nanoscale structures in waveguides. For example, nanoscale structures can manipulate

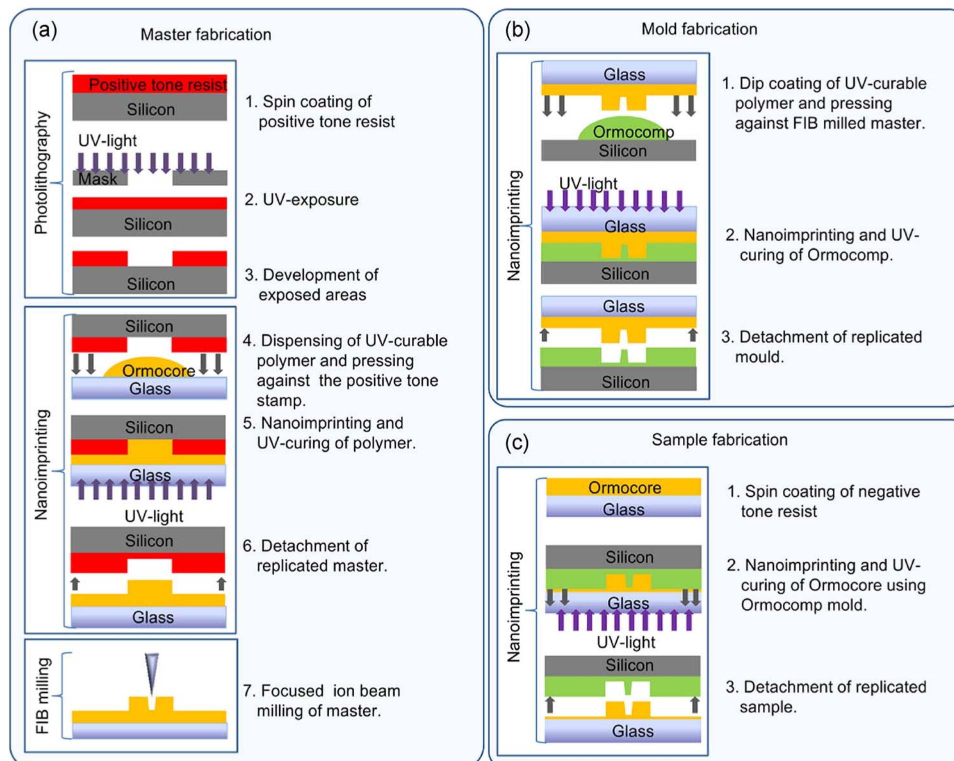

Fig. 1. Main fabrication steps to make nanoslot waveguide. (a) Master fabrication consists of photolithography, nanoimprint, and FIB milling steps. (b) Mold is fabricated by nanoimprinting UV-curable polymer. (c) Nanoslot waveguide is replicated by nanoimprinting mold on spin-coated polymer.

the propagation of the light in a waveguide or influence light coupling properties [7], [8]. For instance, gratings have been used to establish the light coupling into or out from the waveguide. To enhance the light interaction with the ambient, a waveguide structure consisting of a few hundred nanometer-wide slots has been demonstrated [9], [10]. The nanoslot waveguide configuration has an attractive property in simultaneously guiding the light propagation and maintaining a strong light–ambient interaction. This makes various applications possible, for example, optical trapping and sensing [11], [12].

The motivation for this paper was to investigate the fabrication of a NIL master mold for waveguide applications by combining a large-area photolithography process and nanoscale FIB milling. The applicability of modifying a NIL master mold using FIB milling was demonstrated by fabricating centimeter-long Y-branch waveguide devices, which include a nanoscale wide slot embedded in one arm of the branch. Furthermore, the applicability of fabricated waveguide structures for sensor applications was investigated.

2. Simulation and Fabrication

The fabrication of the samples consists of the following three main phases: 1) making the master; 2) fabrication of the replication mold; and 3) nanoimprinting of the waveguide sample. The structures with a size below the diffraction limit were built in the master by combining photolithography, nanoimprint, and FIB milling.

The fabrication of the master involved three steps, which are illustrated in Fig. 1(a). First, the positive tone resist was spin coated on a silicon substrate. The thickness of the positive tone resist

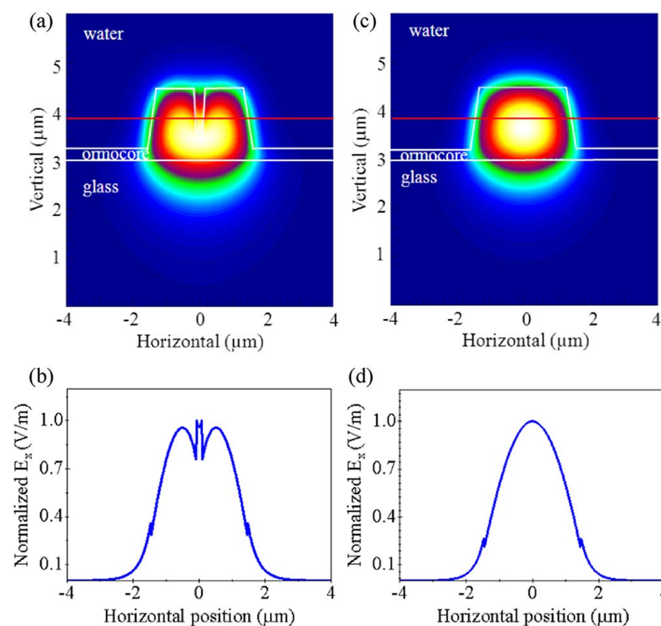

Fig. 2. (a) Electric field E_x profile of TE-mode in the slot waveguide. (b) Cross-sectional plot of the E_x field of TE mode indicated as a red line in (a). (c) Electric field E_x profile of TE-mode in the ridge waveguide. (d) Cross-sectional plot of the E_x field of TE mode indicated as a red line in (c).

layer, which is about 1.3 μm, determines the height of the final waveguide ridge. The resist was photolithographically patterned in order to produce a stamp by exposing UV-light through a shadow mask and removing the exposed areas with a developer. Next, the negative tone resist, i.e., Ormocore, was dispensed on a borofloat glass substrate, and the pattern on the positive tone stamp was replicated on it by imprinting and UV-curing Ormocore resist. The replicated Ormocore master was detached and hardened by post-baking it for 1 h at 130 °C. Then, conductive aluminum coating was vacuum evaporated on the master in order to avoid charge-up of the surface during FIB milling. As the last phase in the master fabrication, nanoscale slots were milled into waveguide templates using the FIB system (FEI Helios Dualbeam 600). The beam current during the milling was 28 pA, and the beam voltage was 30 kV. Three different slot lengths (40, 80, and 120 μm) were milled into the middle of one arm of the Y-branch waveguide master. FIB milling was followed by the removal of the aluminum coating with 10% NaOH solution.

The master was identical with the sample. Therefore, the mold for the sample fabrication was replicated from the master. The mold fabrication phase is shown in Fig. 1(b). First, the master was treated with an antiadhesion coating of (1,1,2,2 H perfluorooctyl)-trichlorosilane. The master was replicated by dispensing resist, Ormocomp, on the silicon wafer, imprinting and UV-curing the replicated mold. The Ormocomp mold utilized to fabricate actual waveguides was released from the master and treated with the antiadhesion coating previously described.

The waveguide sample fabrication illustrated in Fig. 1(c) was started by spin-coating diluted Ormocore (Ormocore: Ma-T1050, 1:7) at 3000 r/min for 60 s on a borofloat glass wafer. The thinner (Ma-T1050) was evaporated at 85 °C for 40 min. Next, the Ormocomp mold was used to replicate the final Y-branch waveguide structures by nanoimprinting and UV-curing the Ormocore resist. Then, the patterned waveguides were hardened by post-baking for 1 h at 130 °C.

The waveguide mode field properties wfere calculated using the finite-element method (FEM) available in the PhotonDesign simulation software [13]. In the simulation, the ambient of the waveguide was considered to be water, which is a typical solution in a sensing application. The refractive indexes (RIs) in the simulation were 1.458 for the borofloat glass wafer, 1.54 for Ormocore, and 1.33 for water at the wavelength of 1305 nm that was used [14]. Fig. 2(a) and (c) shows the lateral electric field E_x distributions of transverse electric (TE) mode in the slot and ridge

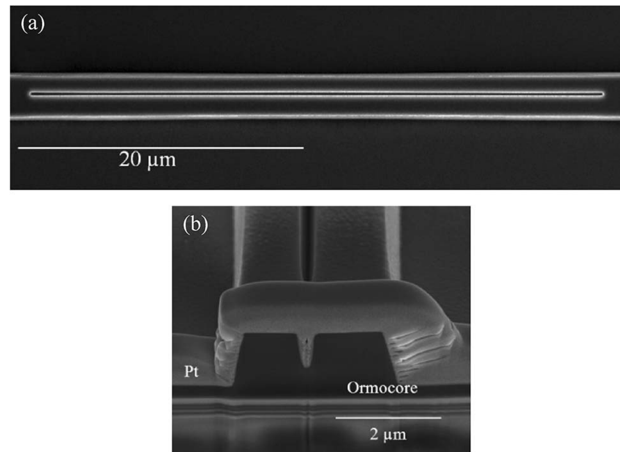

Fig. 3. (a) SEM image from the top of fabricated slot waveguide. (b) Cross-sectional SEM image of the slot part of the waveguide.

waveguides, respectively. The waveguide dimensions for the calculation were achieved from the scanning electron microscope (SEM) image in Fig. 3(b). As shown in Fig. 2(a), the optical field partly propagates in the medium in the slot. The horizontal cross-sectional plots of the E_x fields shown in Fig. 2(b) and (d) illustrate that the maximum of the optical field locates in the water in the slot waveguide and in the core of the ridge waveguide. The E_x field is slightly enhanced in the slot region confirming the slot mode operation. However, this enhancement is low compared with the enhancement achievable with high-index-contrast slot waveguide structures [9].

The interaction of the optical mode with the water ambient in the slot and ridge waveguides was compared by calculating the filling factor for both geometries with the equation

$$f_w = \frac{\int_W P_z(a)da}{\int_W P_z(a)da}. \tag{1}$$

In (1), $P_z(a)$ is a time-averaged Poynting vector, and the numerator is integral over the water region W [15]. The filling factors for a slot waveguide and a ridge waveguide with the same dimensions are 5.1% and 2.5%, respectively. This shows that the optical field of the slot waveguide interacts more with the ambient than the optical field of the ridge waveguide.

The sensitivity of the waveguide against the ambient RI change is often determined as a slope of the linear regression $\Delta n_{mode}/\Delta n_a$, where Δn_{mode} is the modal effective RI change, and Δn_a is the RI change of the ambient [16]. In Fig. 4, the effective RI changes of TE mode in a slot waveguide and a ridge waveguide against the ambient RI are plotted. The ambient RI is shifted from 1.32 to 1.33. Calculated sensitivities are 0.054 and 0.026 for the slot and ridge waveguides, respectively.

3. Characterization

The characterization covered the analysis of the structural and functional properties. The surface roughness of the FIB milled section was determined with an atomic force microscope (AFM). Waveguide transmission measurement was used for optical characterization of the fabricated waveguides. Furthermore, the operation of the Y-branches in interferometric measurement was demonstrated.

Fig. 3(a) shows the SEM image of the fabricated slot waveguide from the top. The horizontal position of the slot in the ridge is constant through the overall length of 40 μm. The width of the photolithography determined ridge is 3 μm. The corresponding cross-sectional SEM image of the slot region is shown in Fig. 3(b). The slot depth is 830 nm, and the width at the top is 340 nm,

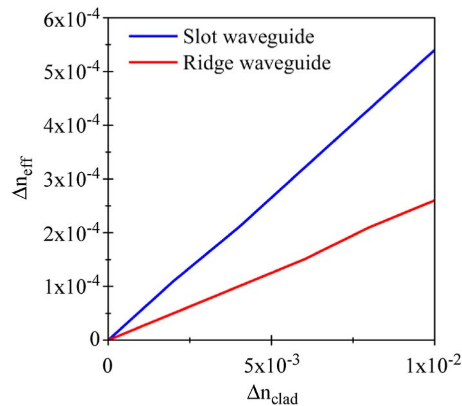

Fig. 4. Effective RI change of TE mode plotted against the RI change of the ambient.

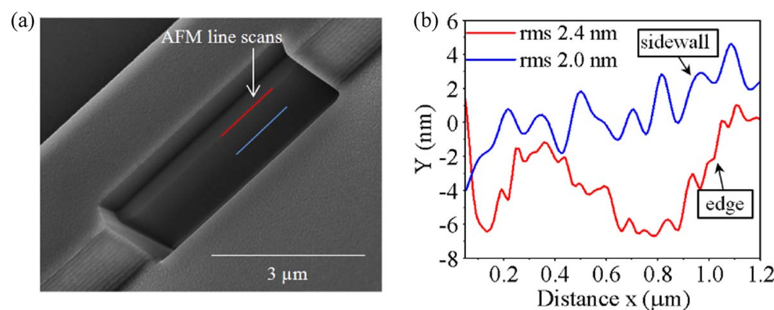

Fig. 5. (a) SEM image of the FIB milled part of the waveguide ridge. The red and blue lines indicate the parts for AFM analysis. (b) Roughness plot of the edge and sidewall region indicated as red and blue lines in (a).

narrowing toward the bottom with a 6.5° angle. The height of the ridge is 1.3 μm. The imprint fabrication method produces a residual layer underneath the replicated pattern. With the process parameters used, the thickness of the residual layer in this paper is about 200 nm.

3.1. Analysis of FIB Milling

In order to investigate the roughness of the FIB milled section, a ridge of the waveguide was milled with FIB using the same parameters as in the master fabrication. The SEM image of the ridge of the waveguide with the FIB milled part is shown in Fig. 5(a). The edge and the sidewall of milled surfaces look smooth. The roughness of the FIB milled part was analyzed by AFM (Veeco Dimension 3100). The root mean square roughness values of the FIB milled edge and the sidewall indicated as a red and blue plot in Fig. 5(b) were 2.4 and 2.0 nm, respectively. Such a small roughness of the edge and the sidewall suggests that FIB milling is a good tool for modifying polymeric molds for waveguides applications.

3.2. Optical Characterization

Transmission of fabricated Y-branch waveguides was analyzed in order to estimate the performance of the slot-embedded waveguide and to evaluate their usability in sensing applications. The transmission measurement setup is illustrated in Fig. 6(a). A laser source operating at a wavelength of 1305 nm was coupled to the polarization-maintaining tapered fiber. The polarization was adjusted with a fiber-optic polarization controller, and the polarization state was verified using an

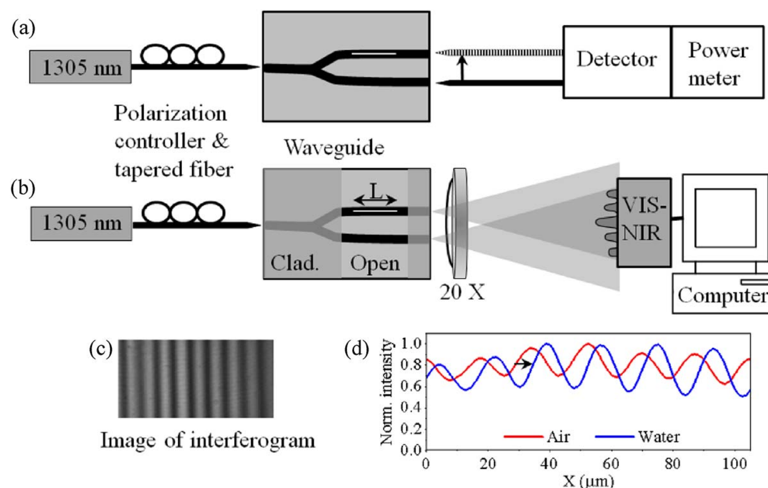

Fig. 6. Schematic of optical characterization methods. (a) Setup for measuring waveguide transmission. (b) Setup for measuring interference of Young interferometry structure. (c) Fringe pattern generated at 700 μm distance on visible-infrared (VIS-IR) camera. (d) Intensity distribution of the interferogram.

external polarizer prior the transmission measurement. The input fiber and the similar output fiber were optimally aligned with the waveguide in order to produce maximum light coupling into the waveguide input facet and from both output arms. The maximum power transmission through the waveguide was measured for both TE and transverse magnetic (TM) polarizations. The average transmissions of eight measured Y-branches were referenced with the fiber-to-fiber power transmission without the waveguide sample between the fibers. The lengths of the Y-branch waveguides were 15 mm. For TE polarization, the average transmission of 31% and 39% were obtained for the slot and reference ridge waveguide arms, respectively. Correspondingly, the average transmission values of 28% and 35% were obtained for TM polarization. These values include the material loss (0.23 dB/cm), coupling losses from the fibers, and the mode coupling loss both in the Y-branch and in the ridge-slot-ridge waveguide interface [14]. From the transmission values measured, the division ratio of the optical power in the slot and ridge waveguide arms was calculated to be 44% and 56%, respectively. The lengths of the slots (40, 80, and 120 μm) in the measured waveguides are too short to enable us to distinguish the transmission loss of the slot waveguide from the other attenuation factors. However, the measured transmission values indicate that the slot waveguide possess good transmission properties.

3.3. Experimental Verification of Slot Mode

The Y-branch waveguide operates as a Young interferometer. The operation is based on the phase difference produced by the two different waveguide arms. One arm of the Young waveguide interferometer was the reference arm, and the other arm consists of a slot with a length of 40, 80, or 120 μm. The operational performance of the Young interferometers with slot waveguides was experimentally verified using the measurement arrangement sketched in Fig. 6(b). The portion of the reference and the sensing arm experiencing the RI variation of the ambient must have the same length in the interference measurement setup used. Therefore, a waveguide sample with an overcladding layer of Ormostamp with a RI of 1.507 was fabricated. The Ormostamp layer was opened for 524 μm $\pm$ 5 μm by using UV-photolithography. The length of the opening determining the sensing area was measured using a white-light interferometer (Wygo, NT3300). The interference measurement was performed for the TE and TM polarizations. The interference pattern was captured with VIS-NIR camera. The output beams of the waveguides were collected by placing a microscope objective with 20$\times$ magnification after the waveguides. Then, the microscope objective was moved 0.7 mm away from the focus in order to acquire the far-field fringe pattern with

TABLE 1

Measured and simulated phase shifts

Device/w Slot length (μm)	Measured phase shift TE polarization	Simulated phase shift TE polarization	Measured phase shift TM polarization	Simulated phase shift TM polarization
0 reference	0.00±0.01	0	0.00±0.01	0
40	1.10±0.01	1.1	0.84±0.01	0.7
80	2.66±0.01	2.3	1.91±0.01	1.4
120	3.68±0.01	3.4	2.32±0.01	2.1

parallel vertical lines. Fig. 6(c) shows an interferogram image on the VIS-NIR camera. The interferogram pattern was video recorded, whereas a water droplet was applied on the opening of Young interferometer. The measured intensity distribution of the interferogram of the Young waveguide structure with a 80-μm-long slot in one arm both with and without water is shown in Fig. 6(d). The phase difference shift is indicated as an arrow in Fig. 6(d).

The intensity of the interferogram picture can be described by the equation

$$I = I_1 + I_2 + 2\sqrt{I_1 I_2}\cos(\Delta\varphi - \delta) \tag{2}$$

where I_1 and I_2 are the intensities of two interfering waveguide beams, and $\Delta\varphi$ is the phase difference of the two beams [17]. The higher fraction of the mode field propagates in the slot and ambient in the slot waveguide, than in the ambient of the ridge reference waveguide. This causes a difference of the effective RI change between the ridge reference arm and the slot waveguide arm at length L of the slot, producing the additional phase shift δ in the fringe pattern. This additional phase shift can be calculated by the equation

$$\delta = 2\pi \frac{L}{\lambda_0} \Delta n_{eff} \tag{3}$$

where $\lambda_0 = 1305$ nm is the wavelength in vacuum and $\Delta n_{eff} = \delta n_{eff}/\delta n_a$ is derivate of the effective RI change in two waveguide arms as the RI of ambient index n_a changes [16]. The phase shift of interference pattern was calculated at the respective spatial period using a fast Fourier transform.

Phase shifts measured and simulated for TE and TM polarizations are shown in Table 1. For the simulation, the effective RI both with air and water ambient in the slot and ridge waveguides were calculated using FEM. The waveguide dimensions for the mode calculation were derived from the cross-sectional SEM image in Fig. 3(b). The effective RI was inserted into equation (2) to calculate the simulated phase shift values. The mode power fraction of TE mode in the slot is higher than in TM mode, causing a bigger phase shift with the TE polarization. The correlation between the measured and the simulated phase shifts is relatively good. The measured values are actually a little higher than the simulated ones. The potential factors for the difference between the measurement and simulation are estimated to be attributed to local waveguide variations such as the residual layer thickness and slot dimension variation.

4. Conclusion

In this paper, we have demonstrated that the FIB milling tool can be used to pattern nanometer scale slot features into the large-dimensional polymeric nanoimprint master mold. SEM and AFM investigations proved that FIB milling provides low surface roughness required in photonic devices. We have also showed that slot waveguides can be nanoimprint fabricated using the FIB modified molds. Proper slot mode propagation was confirmed by interferometric measurements at a wavelength of 1305 nm. Optical analysis also showed that the fabricated slot waveguides possessed good transmission properties.

References

[1] J. L. Guo, "Nanoimprint lithography: Methods and material requirements," *Adv. Mater.*, vol. 19, no. 4, pp. 495–513, Feb. 2007.
[2] H.-W. Sun, J.-Q. Liu, D. Chen, and P. Gu, "Optimization and experimentation of nanoimprint lithography based on FIB fabricated stamp," *Microelectron. Eng.*, vol. 82, no. 2, pp. 175–179, Oct. 2005.
[3] H. D. Wanzenboeck, S. Waid, E. Bertagnolli, M. Muehlberger, I. Bergmair, and R. Schoeftner, "Nanoimprint lithography stamp modification utilizing focused ion beams," *J. Vac. Sci. Technol. B, Microelecton, Nanom. Struct.*, vol. 27, no. 6, pp. 2679–2685, Nov. 2009.
[4] S. Reyntjens and R. Puers, "A review of focused ion beam application in microsystem technology," *J. Micromech. Microeng.*, vol. 11, no. 4, pp. 287–300, Jul. 2001.
[5] J. Hiltunen, M. Hiltunen, J. Puustinen, J. Lappalainen, and P. Karioja, "Fabrication of optical waveguides by imprinting: Usage of positive tone resist as a mould for UV-curable polymer," *Opt. Exp.*, vol. 17, no. 25, pp. 22 813–22 822, Dec. 2009.
[6] M. Wang, J. Hiltunen, S. Uusitalo, J. Puustinen, J. Lappalainen, P. Karioja, and R. Myllylä, "Fabrication of optical inverted-rib waveguides using UV-imprinting," *Microelectron. Eng.*, vol. 88, no. 2, pp. 175–178, Feb. 2011.
[7] M. Hiltunen, L. Dal Negro, N.-N. Feng, L. C. Kimeling, and J. Michel, "Modeling of aperiodic fractal waveguide structures for multifrequency light transport," *J. Lightwave Technol.*, vol. 25, no. 7, pp. 1841–1847, Jul. 2007.
[8] S. Grego, J. R. McDaniel, and B. Stoner, "Wavelength interrogation of grating-based optical biosensors in the input coupler configuration," *Sens. Actuators B, Chem.*, vol. 131, no. 2, pp. 347–355, May 2008.
[9] Q. Xu, V. R. Almeida, R. R. Panepucci, and M. Lipson, "Experimental demonstration of guiding and confining light in nanometer-size low-refractive-index material," *Opt. Lett.*, vol. 29, no. 14, pp. 1626–1628, Jul. 2004.
[10] M. Hiltunen, J. Hiltunen, P. Stenberg, J. Petäjä, E. Heinonen, P. Vahimaa, and P. Karioja, "Polymeric slot waveguide at visible wavelength," *Opt. Lett.*, vol. 37, no. 21, pp. 4449–4451, Nov. 2012.
[11] A. H. J. Yang, S. D. Moore, B. S. Schmidt, M. Klug, M. Lipson, and D. Ericson, "Optical manipulation of nanoparticles and biomolecules in sub-wavelength slot waveguides," *Nature*, vol. 457, no. 7225, pp. 71–75, Jan. 2009.
[12] C. A. Barrios, "Optical slot-waveguide based biochemical sensors," *Sensors*, vol. 9, no. 6, pp. 4751–4765, Jun. 2009.
[13] FimmWave Software Photon Design Ltd., Oxford, U.K.
[14] Datasheet for Ormocore, Microresist Technology. [Online]. Available: http://www.microresist.de/products/ormocers/pdf/pi_ormocore_clad_en_07062201_ls_neu.pdf
[15] T. D. Visser, B. Demeulenaere, J. Haes, D. Lenstra, R. Baets, and H. Blok, "Confinement and modal gain in dielectric waveguides," *J. Lightwave Technol.*, vol. 14, no. 5, pp. 885–887, May 1996.
[16] X. Fan, *Advanced Photonic Structures for Biological and Chemical Detection*. New York, NY, USA: Springer-Verlag, 2009.
[17] B. E. A. Saleh and M. C. Teich, *Fundamentals of Photonics*. New York, NY, USA: Wiley, 1991.